*Proceedings of the 7th International Conference on Fluid Flow, Heat and Mass Transfer (FFHMT'20)*
*~~Niagara Falls, Canada~~ Virtual Conference – November, 2020*
*Paper No. 178*
*DOI: 10.11159/ffhmt20.178*

# Modeling Combustion and Heat Transfer in a Single-Element $GCH_4$/GOX Rocket Combustor

**Christof Roth[1], Nikolaos Perakis[1], Oskar J. Haidn[1]**
[1]Chair of Space Propulsion, Technical University Munich
Boltzmannstr. 15, 85748 Garching, Germany
christof.roth@tum.de; nikolaos.perakis@tum.de

***Abstract*** **-** The present paper focuses on the numerical modeling of the combustion and heat transfer processes occurring in a $GCH_4$/GOX rocket combustor, which was tested experimentally at the Technical University of Munich. A CFD model, using a RANS formulation to resolve the turbulent flow in the combustor, is set up and a grid independence study is performed. Three different combustion models are applied and the results are compared among each other, as well as to the experimental data. The applied models are an equilibrium chemistry model, a non-adiabatic flamelet model, and laminar finite rate chemistry. The models vary in fidelity as well as computational expense. Their ability to resolve the underlying physical processes of the reactive flow in the combustion chamber is investigated and discussed.

***Keywords*****:** CFD, RANS, Combustion Modeling, Rocket Combustor, Methane, Heat Transfer

## 1. Introduction

To reduce the development cost and time of modern liquid rocket engines (LREs), numerical tools are utilized in the design phase to support or even substitute costly test campaigns and avoid excessive over-design and redesign efforts. The legacy design tools available are one-dimensional and empirical, and typically focus on performance. Heat transfer, which is a key driver for thrust chamber designs, is predicted by simple Nusselt correlations. These correlations mostly do not include critical factors such as injector effects or three-dimensionality of the flow field. If included, this is usually done by empirical or semi-empirical corrections, which need to be validated with costly tests and often cannot be transferred to new designs or different combustors [1].

Computational Fluid Dynamics (CFD) is a promising approach to remedy these shortcomings and improve the classic design and optimization strategies for LREs [2]. Instead of relying on empirical correlations, the principle underlying physics are resolved. However, CFD results must be validated against experimental data to improve confidence in their predictive capabilities and check the settings of the employed modeling parameters.

A single element lab-scale rocket combustor, using gaseous methane ($CH_4$) as fuel and gaseous oxygen (GOX) as oxidizer, described by Silvestri et al. [3], is modeled numerically using the commercial CFD code ANSYS Fluent [4]. Turbulent flow is treated by solving the Reynolds Averaged Navier-Stokes Equations (RANS). The computational setup includes several user developed model extensions. While there has been comprehensive research on combustion in hydrogen engines traditionally [5], [6], recent research activities have focused on developing analysis capabilities for methane engines. Methane shows good performance and cooling properties, as well as low-toxicity and space storability and is therefore an attractive option for future space transport systems [7].

## 2. Numerical Model

### 2.1. Fluid Flow Modeling

The flow field in the combustion chamber is described by the conservation equations for mass, momentum and energy in three-dimensional space:

$$\frac{\partial \bar{\rho}}{\partial t} + \frac{\partial (\bar{\rho} \tilde{u}_i)}{\partial x_i} = 0 \tag{1}$$

$$\frac{\partial(\bar{\rho}\tilde{u}_i)}{\partial t} + \frac{\partial(\bar{\rho}\tilde{u}_i\tilde{u}_j)}{\partial x_j} = -\frac{\partial \bar{p}}{\partial x_i} + \frac{\partial}{\partial x_i}(\bar{\tau}_{ij} - \bar{\rho}\widetilde{u_i'' u_j''}) \tag{2}$$

$$\frac{\partial(\bar{\rho}\tilde{h})}{\partial t} + \frac{\partial(\bar{\rho}\tilde{h}\,\tilde{u}_i)}{\partial x_i} = \frac{\partial}{\partial x_i}\left(\frac{\bar{\lambda}}{\bar{c}_p}\frac{\partial \tilde{h}}{\partial x_i} - \bar{\rho}\widetilde{u_i'' h''}\right) \tag{3}$$

where $\bar{\rho}$ and $\bar{p}$ are the Reynolds-averaged density and pressure respectively and $\tilde{u}_i$ are the Favre-averaged velocity components in the spatial directions $x_i$. The viscous stress tensor is $\bar{\tau}$. The absolute specific enthalpy is $\tilde{h}$, $\bar{c}_p$ and $\bar{\lambda}$ are the specific heat and the thermal conductivity of the fluid.

A pressure-based scheme is used for the solution of the discretized equations. Density and pressure are coupled through the ideal gas equation of state.

### 2.2. Turbulence Modeling

Reynolds-averaging of the Navier-Stokes equations introduces unclosed terms in the momentum and energy equations, which need to be closed with an appropriate turbulence model. The turbulent momentum flux is modeled employing the Boussinesq hypothesis, relating the Reynolds stresses to the mean velocity gradients.

Turbulent closure is achieved by employing the standard k-$\varepsilon$ model proposed by Launder and Spalding [8] and using a two-layer approach for the wall. The model allows for the determination of the turbulent length and time scales by solving two additional transport equations for turbulent kinetic energy $\tilde{k}$ and its dissipation $\tilde{\varepsilon}$. The turbulent viscosity and model parameters are set as proposed in the standard model.

The near wall region is treated with a zonal approach depending on the resolution of the boundary layer. Where the computational grid resolves the viscosity-affected region, a one-equation model by Wolfshtein [9] is employed, otherwise, wall functions are used to bridge the region between the fully developed flow and the wall. Blending functions are employed for smooth transitions between the different regions.

The closure of the turbulent heat flux in Equation (3) is achieved employing a turbulent Prandtl number of 0.9 throughout the domain.

### 2.3. Combustion Modeling

The combustion processes occurring in the thrust chamber must be modeled accurately for a reliable prediction of the heat transfer to the wall. This includes the initial heat release in the flame zone as well as the post-flame recombination reactions in the strongly cooled boundary layer. Three different approaches are compared here. The first one is built on the assumption of infinitely fast chemistry, i.e. local reaction to equilibrium. It has been applied successfully in rocket combustion modeling of $H_2/O_2$ engines [6], [10]. Its applicability is questionable for hydrocarbon fuels however, due to the comparatively larger time scales of the chemical reactions involved. Therefore, a second approach based on a newly developed non-adiabatic flamelet model incorporating non-equilibrium effects is also employed. Both these approaches use pre-processed chemistry tables to look up thermochemical variables and transport properties during runtime. The third approach resolves the chemical reactions by including finite rate chemistry, employing a chemical kinetic scheme based on Arrhenius reaction rate theory. This approach is thought to have the highest modeling fidelity, but is also very expensive in terms of computational cost and tends to be numerically more demanding as it deals with stiff chemical systems.

#### 2.3.1. Tabulated Chemistry Models

The combustion in a LRE depends directly on the mixing process, driven by the injector design, and the underlying chemistry of the propellant combination. The relative speed of the chemical reactions compared to the mixing progress is critical for the choice of the employed modeling approach and is described by the Damköhler number $Da = \tau_{mix}/\tau_{chem}$, where $\tau_{mix}$ is a representative mixing time scale and $\tau_{chem}$ a representative chemical time scale.

For flows with high Damköhler numbers (Da>>1) the reaction progress is limited by turbulent mixing. This can be used to reduce the combustion process to a mixing problem and decouple the thermochemistry from the turbulent flow. Thermochemical variables as well as transport properties can then be stored in lookup-tables which are evaluated during the the solution of the fluid flow. This negates the need for time-consuming computation of stiff chemical systems during the the solution process. Additionally thermochemistry is reduced to a single parameter called the mixture fraction, which is is defined as the mass fraction originating from the fuel inlet stream:

$$\mathrm{Z} = \frac{Z_i - Z_{i,Ox}}{Z_{i,Fu} - Z_{i,Ox}} \tag{4}$$

where $Z_i$ is the elemental mass fraction of the chemical element $i$ and the subscripts Ox and Fu denote values originating from oxidizer or fuel streams respectively.

Instead of solving one transport equation for every chemical species occurring, now only one for the mixture fraction has to be solved:

$$\frac{\partial(\bar{\rho}\tilde{Z})}{\partial t} + \frac{\partial(\bar{\rho}\tilde{Z}\,\tilde{u}_i)}{\partial x_i} = \frac{\partial}{\partial x_i}\left(\frac{\mu + \mu_t}{Sc_t}\frac{\partial \tilde{Z}}{\partial x_i}\right) \tag{5}$$

where $Sc_t$ is the turbulent Schmidt number introduced in analogy to the turbulent viscosity for modeling the turbulent mixture fraction transport. Here the Schmidt number is set to a constant value of $Sc_t = 0.6$ throughout the domain.

In the most general case, all tabulated variables are stored as a function of five independent variables:

$$\tilde{\phi} = f(\tilde{Z}, \widetilde{Z''^2}, \tilde{h}, \bar{p}, \tilde{\chi}) \tag{6}$$

where $\widetilde{Z''^2}$ is the mixture fraction variance and $\tilde{\chi}$ is the scalar dissipation.

When employing the equilibrium chemistry model (ECM), tables are generated using NASA's Chemical Equilibrium with Applications code [11]. CEA uses a minimization of free energy method to calculate the equilibrium composition, which makes it possible to treat species independently in the algorithm without specifying a chemical kinetic scheme a priori. The condition for chemical equilibrium is stated in terms of Gibbs free energy. When this approach is employed, the influence of scalar dissipation on the flow is assumed to be negligible, i.e. $\chi = 0$.

When employing the flamelet approach, the tables are generated using the method developed by Perakis et al. [12]. This approach generates flamelet tables by solving the governing equations of a counterflow diffusion flame in mixture fraction space. To model the effect of heat loss in the cooled boundary layer the approach includes the dependency of the mixture composition on enthalpy. Non-equilibrium effects are included through tabulation dependent on the scalar dissipation:

$$\tilde{\chi} = \frac{\mathrm{C}_\chi \tilde{\varepsilon} \widetilde{Z''^2}}{\tilde{\mathrm{k}}} \tag{7}$$

where $\mathrm{C}_\chi$ is a constant with value of 2.0. Note that the scalar dissipation therefore depends on the variance and vanishes in regions with no mixture fraction variance. An additional transport equation is solved for the evaluation of the mixture fraction variance field.

#### 2.3.1. Species Transport Chemistry Models

When employing finite rate chemistry to resolve the combustion process the following conservation equation must be solved for every appearing chemical species $k$:

$$\frac{\partial(\bar{\rho}\tilde{Y}_k)}{\partial t} + \frac{\partial(\bar{\rho}\tilde{Y}_k\,\tilde{u}_i)}{\partial x_i} = \frac{\partial}{\partial x_i}\left(\left[\bar{\rho}D_k - \frac{\mu_t}{Sc_t}\frac{\partial \tilde{Y}_k}{\partial x_i}\right]\right) + \dot{\omega} \tag{8}$$

where $Y_k$ is the mass fraction of the k[th] species, $D_k$ the mass diffusion coefficient, $Sc_t$ is the turbulent Schmidt number with a constant value of 0.6 and $\omega_k$ is the net rate of production of species $k$. In accordance with the tabulated chemistry models the mass diffusion coefficient is determined by assuming a unity Lewis number. The net production rate of the species $k$ is determined by the sum of the production rates of that species over all occurring reactions. The reaction rate constants are obtained from the classical Arrhenius equation. For the simulations presented the methane oxidation scheme by Sankaran et al. [13] is used. The scheme includes 16 species and 72 reactions.

## 3. Experimental Setup and Test Data

The experimental combustor investigated here has been tested by the Technical University of Munich as part of the research program SFB-TRR40 "Technological Foundations for the Design of Thermally and Mechanically Highly Loaded Components of Future Space Transportation Systems". It has been designed as part of a larger effort to support the verification and validation of numerical tools for the design of rocket injectors and combustors.

The experiment reported by Silvestri [3] was run at several different operating point distinct by their chamber pressure $p_c$ and their oxidizer to fuel ratio $O/F$. To characterize the performance and the heat transfer of the combustor assembly pressure and temperature measurements were taken in axial direction along the combustor wall. A schematic of the combustion chamber assembly is shown in Figure 1.

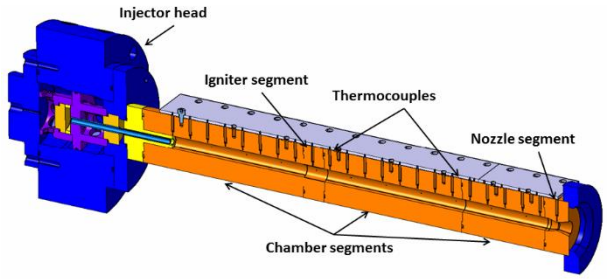


Fig. 1: Combustion chamber assembly.

The combustor uses gaseous oxygen as oxidizer and gaseous methane as fuel. The propellants are injected into the combustion chamber through a single shear-coaxial injector element on the symmetry axis. The oxidizer post has a diameter of 4 mm and the fuel annulus an inner diameter of 5 mm and an outer one of 6 mm. In the investigated configuration, the oxidizer post is flush mounted with faceplate and no tapering is applied.

The circular combustion chamber is lab-scale, with a length of 305 mm and an inner diameter of 12 mm. The throat diameter of the convergent-divergent nozzle is 7.6 mm. The chamber is a heat sink design made of oxygen free high conductivity copper. It is capacitively cooled only. Wall temperatures have been measured in the cylindrical part using thermocouples. The thermocouples are clustered in pairs of three, with a distance on 1, 2 and 3 mm from the hot gas wall respectively. This is done to reconstruct the heat flux from the thermocouple readings using an inverse heat transfer method presented by Perakis et al. [14]. Pressure transducers are integrated along the combustor wall for the evaluation of the axial pressure distribution.

## 4. Numerical Investigation

### 4.1. Grid Study

In order to get an estimation of the discretization error, i.e. the difference between the converged solution on a specific specific grid and the 'exact' solution, the grid convergence index (GCI) according to the procedure proposed by Roache [15] Roache [15] is evaluated. Iterative convergence is achieved by reducing the normalized residuals for each equation solved solved by at least four orders of magnitude. Two grids, varying in the number of computational cells, were generated for this study. The fine grid (grid f) consist of 91735 cells, the medium grid (grid m) of 54189 cells. Calculations with three different discretization schemes are conducted for both grids. The applied schemes are, a first order upwind scheme, a second order upwind scheme, and a third order MUSCL scheme. All calculations are performed using the ECM as baseline for simulating the combustion processes. As critical design parameter for the heat management system in LREs, the integrated wall heat flux is chosen as key variable for judging global grid convergence. The results of the calculation for the discretization error based on the wall heat flux are given in Table 2. The numerical error is calculated by comparing the solutions on each grid to a value gained from Richardson.

Table 2: Estimation of discretization error.

| | | Grid | 1st Order | 2nd Order | 3rd Order |
|---|---|---|---|---|---|
| Q | [kW] | m | 93 | 97 | 97 |
| | | f | 94 | 98 | 98 |
| | | ext | 99 | 98 | 98 |
| GCI | [%] | m | 24.2 | 4.6 | 3.7 |
| | | f | 7.8 | 1.1 | 0.7 |

The extrapolated values for the different schemes only differ by around one percent. For the following mainly qualitative investigations, as well as the experimental data at hand for validation, a numerical error less than 10% was deemed adequate. All simulations were calculated on the fine grid. All simulations using ECM or NAF as combustion models were calculated with the 2nd order scheme, while for the FRC the 1st order scheme had to be used due to convergence difficulties.

### 4.2. Combustion Model Studies

The design of the injector elements used in a LRE has a direct impact on the engines performance and thermal environment, as it is the main driver for mixing efficiency in the system. The primary measure of the rocket engine performance related to the injection system is the characteristic velocity $c^*$, which describes the basic impulse of the engine prior to expansion, but beyond choked conditions in the nozzle throat. The characteristic velocity is defined as:

$$c^* = \frac{p_c A_{th}}{\dot{m}} \tag{9}$$

where $p_c$ is the stagnation pressure at the throat, $A_{th}$ is the throat area and $\dot{m}$ the total mass flow rate of oxidizer and fuel combined. Therefore, the characteristic velocity defines the throat area needed to achieve a certain chamber pressure at a given mass flow rate. For a 'perfect injector' the characteristic velocity is mainly a function of the propellant combination. A 'perfect injector' is characterized by mixing, evaporating and reacting the propellants to equilibrium before entering the thrust chamber.

The combustion efficiency of a rocket combustor can then be defined as the ratio of the characteristic velocity of the real injector compared to the characteristic velocity of the 'perfect' or 'ideal injector':

$$\eta_{c^*} = \frac{c^*}{c^*_{id}} \tag{10}$$

Here the characteristic velocity for the ideal system is determined using NASA's CEA code [12]. One of the of the calculation of theoretical rocket performance in CEA is adiabatic combustion. When dealing with substantial heat through the combustor wall this assumption is no longer valid. The energy is leaving the system and does not contribute rising the chamber pressure. This is taken into account in this study by subtracting the integrated heat flux up to the from the injection enthalpy of the propellants, when calculating the ideal characteristic velocity. This results in the non-adiabatic combustion efficiency $\eta^*_{c,h}$.

The results for all studied cases as well as the experiment are comprised in Table 3.

Table 3: Calculated combustion efficiency

| | | Experiment | ECM | FRC | NAF |
|---|---|---|---|---|---|
| $\eta^*_c$. | [%] | 92.8 | 87.6 | 92.2 | 90.1 |
| $\eta^*_{c,h}$. | [%] | 98.6 | 100.6 | 99.4 | 101.2 |

Note that in general the combustion efficiency is less than 100%. However, in some cases the energy released can be greater for a system not in chemical equilibrium, or a certain stratification of temperature and velocity can give higher than fully mixed performance [16]. In addition, secondary effects like the initial momentum of the propellants at the injector and the momentum boundary layer are not corrected for here. This can explain the high values for the simulated cases. In any case all simulations show a high combustion efficiency, i.e. a good mixing characteristic of the injector.

Figure 5 shows the pressure along the combustor wall predicted by the different combustion models in comparison with the experimental data. A total error of 2% is also shown for the experiment. This value is not derived from error analysis and only included for reference. The ECM and the NAF model underestimate the wall pressure significantly, while the FRC is within 2% of the experimental values for all data points.

The differences in the wall pressure distributions can be explained by looking at the wall heat flux curves given in Figure 6. As expected the curves show an opposite trend compared to the wall pressure distribution, confirming the previously mentioned relation between pressure buildup and heat loss. The ECM predicts the highest heat flux followed by the NAF. Both show significantly higher values than the FRC and the experimental data. The FRC is just outside of a 15% error, assumed for the experiment, for most of the chamber.

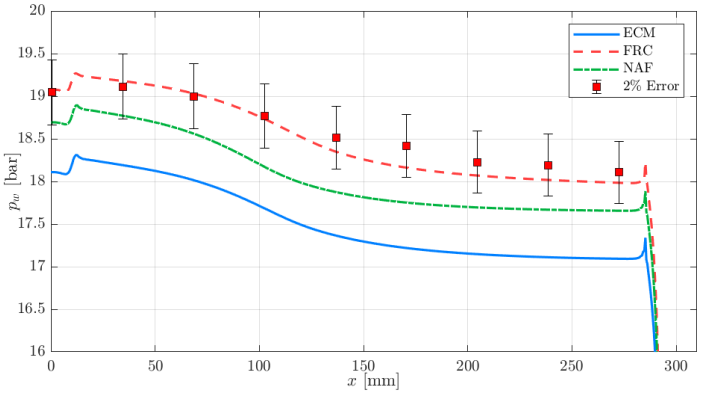


Fig. 5: Wall pressure.

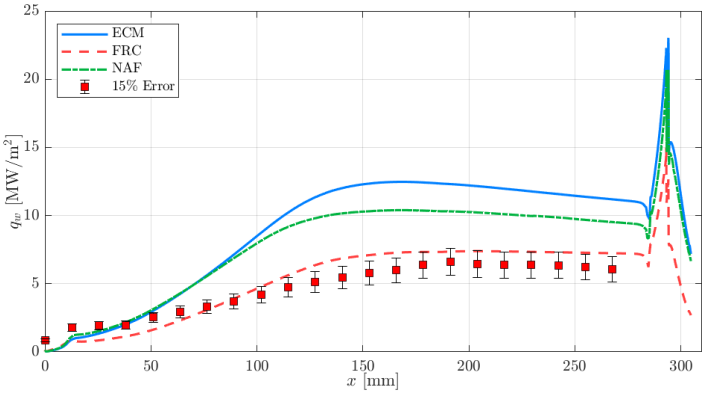


Fig. 6: Wall heat flux.

The reason for the comparatively low heat flux in case of the FRC model can be observed in Figure 7, where the hot gas main product mass fractions along an evaluation line located at x=250 mm are shown. While the ECM and the NAF predict a decrease of CO of approximately 45% and an increase of $CO_2$ of 30% in the region roughly 1.5 mm close to the wall, the composition is practically frozen in case of FRC. This difference is the main driver for the higher heat

flux predicted by ECM and NAF, where the recombination energy of the CO- $CO_2$ balance is released in the wall near region. Reactions in the FRC model are mainly driven by the presence of radicals. As the present radicals decrease in amount towards the wall, reactions slow down and the composition becomes frozen. As an indicator, the OH mass fraction is given in Figure 8. In the presented case, OH was the most prevalent radical.

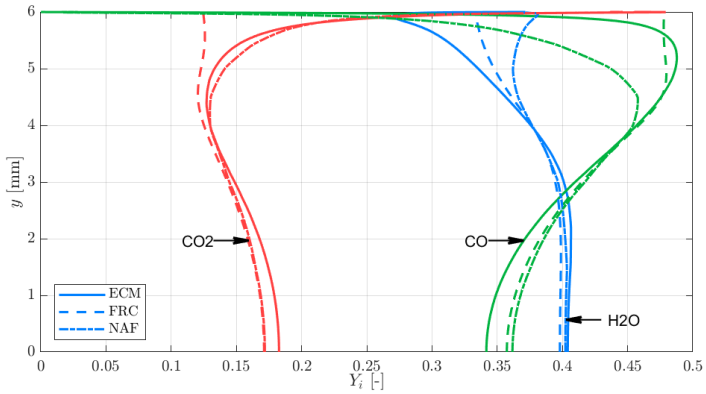


Fig. 7: Main combustion products along evaluation line.

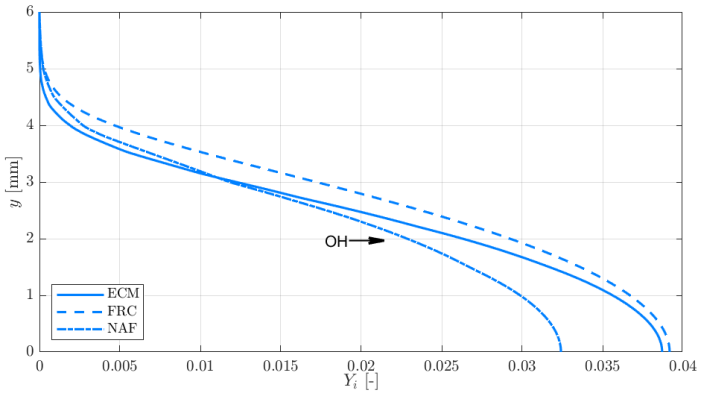


Fig. 8: OH radical mass fractions along evaluation line.

Looking at the average temperature along the combustor given in Figure 9, FRC and NAF actually predict higher values compared with the ECM model. However, this is only true for the mean. The temperatures of the wall adjacent cells are highest for the ECM and display the same qualitative trend as the wall heat flux, see Figure 10. Along the crossection at an evaluation point of x=250 mm it can be seen, that, as the enthalpy defect increases towards the wall and the mixture enthalpy deviates from the adiabatic value. The temperatures found in chemical equilibrium are higher compared to the temperatures predicted by the NAF and the FRC, leading to a higher heat transferred to the wall.

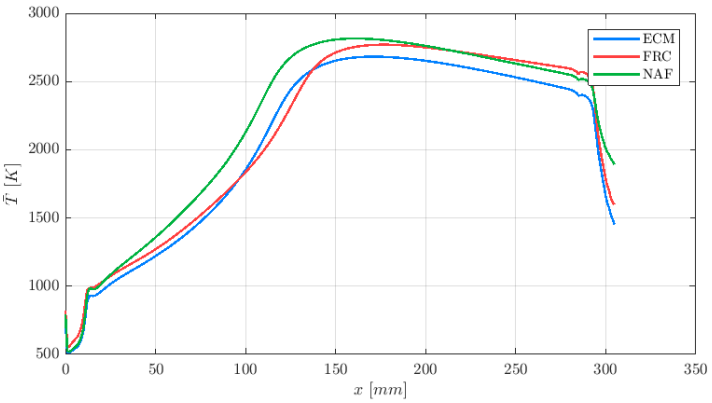


Fig. 9: Cross-sectional-averaged temperature.

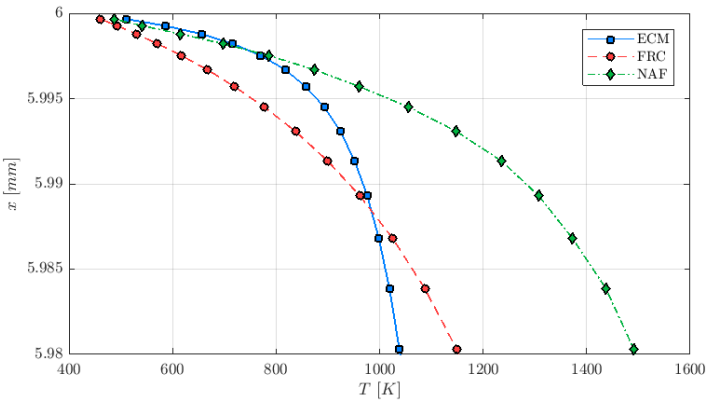


Fig. 10: Near wall temperature along evaluation line.

## 5. Conclusion

Three different combustion models have been evaluated for their feasibility to be used in the simulation of a single-element $GCH_4$/GOX rocket combustor. One was based on the assumption of chemical equilibrium, one based on finite rate chemistry with an underlying chemical kinetic scheme. The third one was based on a recently developed non-adiabatic flamelet approach.

Only the finite rate chemistry model showed acceptable agreement with the experimental data in terms of pressure and heat flux distribution. The discrepancies in the results produced by the equilibrium and the flamelet model mainly stem from an over-prediction of the recombination processes of the CO-$CO_2$ balance in the strongly cooled boundary layer. While the

finite rate chemistry approach predicts an almost frozen composition close to the wall after the amount of radicals present in the mixture becomes negligible, CO still decreases by approximately 45% and $CO_2$ increases by 30% in case of equilibrium and flamelet.

The finite rate chemistry model however is much more computational expensive and prone to instable convergence compared to the other two models as it does not implement a tabulation routine and needs to solve several additional transport equations for species as well as dealing with stiff chemistry systems. This makes it prohibitive to be used in design phases, where quick turnaround times are needed, especially when considering more complex sub- or full-scale engines.

To improve the results of the tabulated chemistry models, a new method, based on knowledge transfer from the higher fidelity finite rate chemistry and taking into account the kinetic effects in the cooled boundary layer, is currently in development at the Technical University of Munich.

## References


[1] J. Lin, J. S. West, R. W. Williams, P. K. Tucker and J. D. Chenoweth, "CFD Code Validation of Wall Heat Fluxes for a $GO_2/GH_2$ Single Element Combustor," in *Proceedings of the 41st AIAA/ASME/SAE/ASEE JPC & Exhibit*, Tucson, AZ, 2005.

[2] O. Knab, A. Fröhlich, J. Görgen and D. Wiedmann, "Advanced Thrust Chamber Layout Tools," in *Proceedings of the 4th International Conference on Launcher Technology*, Liege, Belgium, 2002.

[3] S. Silvestri, "Investigation on Heat Transfer and Injector Design Criteria for Methane/Oxygen Rocket Combustion Chambers," Dissertation, Technical University of Munich, Germany, 2019.

[4] ANSYS Inc., "18.0 ANSYS Fluent Theory Guide 18.0," 2018.

[5] P.K. Tucker, S. Menon, C.L. Merkle, J.C. Oefelein and Vigor Yang, "Validation of High-Fidelity CFD Simulations for Rocket Injector Design," in *Proceedings of the 44th AIAA/ASME/SAE/ASEE JPC & Exhibit*, Hartford, CT, 2008.

[6] H. Riedmann, B. Kniesner, M. Frey and C.D. Munz, "Modeling of combustion and flow in a single element $GO_2/GH_2$ combustor," *CEAS Space Journal*, 2014.

[7] H. Burkhardt, M. Sippel, A. Herbertz and J. Klevanski, "Kerosene vs. Methane: A Propellant Tradeoff for Reusable Liquid Booster Stages," *Journal of Spacecraft and Rockets*, 2004.

[8] B. E. Launder and D.E. Spalding, *Mathematical models of turbulence*. London-New York: Academic Press, 1973.

[9] M. Wolfshtein, "The Velocity and Temperature Distribution of One-Dimensional Flow with Turbulence Augmentation and Pressure Gradient," *International Journal of Heat and Mass Transfer*, 1969.

[10] B. Ivancic, H. Riedmann and M. Frey, "Validation of turbulent combustion models for 3D-simualtions of liquid H2/O2 rocket combustors," in *Proceedings of the Space Propulsion Conference*, Bordeaux, France, 2012.

[11] B. J. McBride and S. Sanford., "Computer Program for Calculation of Complex Chemical Equilibrium Compositions and Applications," NASA RP 1311, 1996.

[12] N. Perakis, C. Roth and O.J. Haidn, "Development of a non-adiabatic Flamelet model for reacting flows with heat loss," in *Proceedings of the Space Propulsion Conference*, Sevilla, Spain, 2018.

[13] R. Sankaran, E.R. Hawkes, J. H. Chen, T. Lu and C.K. Law, "Structure of a spatially developing turbulent lean methane-air Bunsen flame," in *Proceedings of the Combustion Institute*, 2007.

[14] N. Perakis, M. P. Celano and O.J. Haidn, "Heat flux and temperature evaluation in a rectangular multi-element GOX/GCH4 combustion chamber using an inverse heat conduction method," in *7th EUROPEAN CONFERENCE FOR AERONAUTICS AND AEROSPACE SCIENCES (EUCASS)*, Mila, Italy, 2017.

[15] P.J. Roache, "Perspective: A Method for Uniform Reporting of Grid Refinement Studies," *Journal of Fluids Engineering*, 1994.

[16] Chemical Propulsion Information Agency, "JANNAF Rocket Engine Performance Prediction and Evaluation Manual," Johns Hopkins University, Laurel, MD, 1975.